Photodissociation of CD_3SCD_3 on the First Absorption Band: Translational and Internal Energy Transfer to the CD_3 Fragment Studied by Resonant Multiphoton Ionization and Time-of-Flight Spectrometry†

Bruno Martínez-Haya*

Departamento de Química Física I, Facultad de Química, Universidad Complutense, 28040 Madrid, Spain, and Departamento de Ciencias Ambientales, Universidad Pablo de Olavide, 41013 Sevilla, Spain

F. J. Aoiz, Luis Bañares,* Pablo Quintana, and Enrique Verdasco

Departamento de Química Física I and CAI de Espectroscopía, Facultad de Química, Universidad Complutense, 28040 Madrid, Spain

Received: March 21, 2000; In Final Form: May 4, 2000

The photodissociation of deuterated dimethyl sulfide (CD_3SCD_3) has been studied in the first absorption band at a laser wavelength of 229 nm. The resonance-enhanced multiphoton ionization time-of-flight technique has been employed to determine the recoil energy distribution and the anisotropy parameter β and to study the rovibrational state population of the nascent CD_3. The observed value $\beta = -0.9 \pm 0.1$ (perpendicular dipole transition) corroborates the C_{2v} $^1B_1$ (or C_s $^1A''$) symmetry of the excited state accessed at 229 nm, as assigned previously by different groups. For dissociation yielding vibrationless CD_3, the center-of-mass translational energy is, on average, 80% of the maximum energy available. $CD_3(v=0)$ fragments are produced with a rotational distribution showing a maximum at $N'' = 9-11$. Evidence for activity of the ν_1 symmetric stretching mode of CD_3 is also observed. These results are compared with those obtained for deuterated methyl iodide (ICD_3).

I. Introduction

Dimethyl sulfide (DMS) has attracted the attention of scientists during the past decades, largely due to its implication in the tropospheric sulfur cycle.[1−3] In particular, the enhancement of DMS oxidation upon irradiation with ultraviolet (UV) light[3] has motivated a series of detailed photodissociation studies.[4−8] Several experiments of this kind were performed in the early 1990s by Lee et al.[7] using molecular beam translational spectroscopy and by Nourbakhsh et al.[6] employing, additionally, photoion−photoelectron coincidence spectroscopy. These experiments, which focused on the 193 nm photodissociation of CH_3SCH_3, confirmed C−S bond breaking as being the dominant channel taking place upon UV absorption, and showed that a substantial part of the energy available (about 60%) is transferred into translational energy of the CH_3 and CH_3S photoproducts. Furthermore, both fragments were found to be scattered without any preferential recoil direction and this was interpreted as being a consequence of the many excited states involved in the photodissociation of this molecule at 193 nm.

We have recently undertaken the study of the photodissociation of DMS following laser excitation at longer wavelengths (227−229 nm).[8] The absorption at these wavelengths is dominated by the first dipole allowed transition in C_{2v} symmetry, $1^1B_1(9a_1 \leftarrow 3b_1) \leftarrow X^1A_1$.[1,9−12] Therefore, one electron in the highest occupied molecular orbital (HOMO) in the ground-state configuration, the $3b_1$ nonbonding orbital, which is essentially the $3p_x$ atomic orbital of sulfur perpendicular to the C−S−C plane,[9] is promoted to the weakly bonding $9a_1$ sulfur 4s Rydberg orbital.

Similarly to the H_2S molecule, the photodissociation of DMS on the first absorption band entails, at least, a second 1^1A_2 electronic state which couples strongly with the 1^1B_1 state. Manaa and Yarkony[13] have recently investigated in extensive electronic calculations the role of nonadiabatic vibronic transitions during the process of DMS photodissociation. Only the $1^1B_1 \leftarrow X^1A_1$ valence−Rydberg transition is symmetry allowed by one photon. In principle, the 1^1B_1 state does not correlate with the ground state fragments $CH_3(X^2A''_2) + CH_3S(X^2\ E)$. However, upon C−S bond breaking, the C_{2v} symmetry relaxes to C_s symmetry and the two lowest-lying excited 1^1B_1 and 1^1A_2 states become $1^1A''$ and $2^1A''$. The lower of these two adiabatic potential energy surfaces (PES) ($1^1A''$) upon stretching of the S−C bond is repulsive and correlates with ground state fragments, whereas the upper PES ($2^1A''$) is binding. The coupling of both $^1A''$ PESs gives rise to conical intersections for nuclear configurations within the Franck−Condon region of the electronic ground state.[13]

In a recent work, we reported on the photodissociation of CH_3SCH_3 at 227.5 nm in a molecular beam.[8] In that study, the CH_3 fragments were detected by 2+1 resonance-enhanced multiphoton ionization (REMPI) through the $3p_z\ ^2A''_2 \leftarrow X^2A''_2$ and $4p_z\ ^2A''_2 \leftarrow X^2A''_2$ Rydberg transitions. The vibronic spectrum corresponding to the ν_2 "umbrella" mode of CH_3 was measured and products in excited states up to $v_2 = 4$ were detected. In addition, from the analysis of the $4p_z$ rotationally resolved 0_0^0 band of CH_3, rotational temperatures were obtained. One main conclusion of this work was that only ≈5% of the total energy available for dissociation was channeled into the internal degrees of freedom of the methyl fragment.

* Corresponding authors. E-mail: banares@legendre.quim.ucm.es.
† Part of the special issue "C. Bradley Moore Festschrift".

10.1021/jp001064z CCC: $19.00
Published on Web 07/12/2000

In the present paper, we report on an extension of the previous study on the photodissociation of DMS through the first absorption band. In this case, we have chosen the fully deuterated isotopomer of the molecule CD_3SCD_3, hereafter DMS-d_6, since the accessible $3p_z$ and $4p_z$ Rydberg states of CD_3 via 2+1 REMPI show a significantly smaller predissociation in comparison with CH_3.[14] Thus, careful analysis of the rotationally state-resolved spectra can yield more reliable data about the energy disposal into the fragments. In addition, we have investigated the amount of the available energy after excitation which appears as translational energy of the fragments and the anisotropy parameter of the photodissociation process by measuring time-of-flight (TOF) profiles of the CD_3 fragments at different polarizations of the pump and probe lasers.

The paper is organized as follows. Sections II and III are dedicated to a brief description of the experimental setup and data analysis employed in this study, respectively. The results are shown and discussed in section IV and the most relevant conclusions are presented in section V.

II. Experimental Section

The REMPI-TOF apparatus employed in the present experiments is an upgraded design of the setup employed in earlier investigations.[8,15]

A pulsed free jet of CD_3SCD_3 (Aldrich, 99.0% D atom) was formed by expanding 170 Torr of pure DMS-d_6 vapor through a pulsed valve (nozzle diameter 0.4 mm, 300 μs aperture time gate) at room temperature. Additional experiments were also carried out with a free jet of pure ICD_3 (Aldrich, 99.5% D atom) under similar conditions at a stagnation pressure of 140 Torr.

The laser radiation interacts with the parent molecule and the photofragments 53 mm downstream along the flow axis of the expanding jet at the midpoint between the ion repeller and extraction plates of a Wiley−McLaren type ion source. These plates are separated by a distance of 1 cm and are followed by a (grounded) acceleration plate at 1 cm from the extractor. The ion source was operated under space-focusing conditions by applying acceleration, E_{acc}, and extraction, E_{ext}, electric fields satisfying the ratio $E_{acc}/E_{ext} \approx 4$. Typical fields were $E_{ext} = 80$ V/cm and $E_{acc} = 320$ V/cm. In some experiments, higher voltages were used, still maintaining the space-focusing conditions, but no effects on the measured spectra were observed. The system of plates accelerates the photoions at 90° with respect to the jet axis toward the detection chamber which hosts the time-of-flight tube (20 cm field-free flight path) and the microchannel plate detector (Hamamatsu F2225-21S, 42 mm diameter). The ionization and detection chambers are evacuated by turbomolecular pumps keeping working pressures during the experiments below 5×10^{-6} mbar.

The pulsed UV laser beam used for dissociation ($\lambda_{pump} =$ 229 nm) was produced in a Nd:YAG-dye system (Quanta-Ray PRO-200/Continuum ND60) operated with LDS698 dye. The 687 nm dye fundamental was doubled to 343.5 nm in a KDP crystal and both wavelengths were mixed in a BBO crystal to produce up to 1 mJ/pulse of the third harmonic 229 nm. A separate Nd:YAG dye laser system (Continuum NY81−20/ND60), operated with an optimized mixture of Rhodamines 590 and 610, was used to probe the CD_3 fragments by 2+1 REMPI through the $4p_z\ ^2A''_2$ Rydberg state ($\lambda_{probe} = 285.7-287.0$ nm). The wavelength of the probe laser can be automatically scanned using an auto-tracking system. Both lasers have time and frequency widths of 6 ns and ≈0.1 cm^{-1}, respectively, and are linearly polarized. The pump and probe lasers were attenuated to 0.1 mJ/pulse and 0.3 mJ/pulse, respectively, for the experiments. With the aid of fast photodiodes, the measured REMPI ion signal was normalized with the pump (linearly) and probe (quadratically) pulse intensities (see below), which remained constant within 10% during each scan.

The pump and probe laser beams were sent counterpropagating into the detection chamber using two separate mirror systems and were focused using 50 and 25 cm focal length lenses, respectively, at the intersection point with the supersonic jet. The polarization direction of the lasers could be oriented in the plane defined by the supersonic jet and the detector axis using achromatic double Fresnel Rhomb prisms. For the wavelength scans of the present REMPI measurements, the pump laser polarization was maintained perpendicular to the TOF axis, while the probe laser polarization was fixed at 54.7° (magic angle) with respect to the pump polarization. A series of experiments with different orientations of the probe laser polarization were performed in an attempt to detect angular momentum alignment in the CD_3 fragments. The angle of the probe laser polarization did not have any detectable effect on the relative intensity of the rotational branches of the CD_3 REMPI spectrum, or on the shape of the TOF profiles of the fragments measured on the Q branch of CD_3 (see section IV).

The experiments with ICD_3 were performed with a single laser, which dissociates the parent molecule and also ionizes the CD_3 fragments by 2+1 REMPI ($\lambda_{pump} = \lambda_{probe} = 285.7-287$ nm). In this case, the laser polarization was kept parallel to the TOF axis and it was possible to resolve the contributions to the CD_3^+ yield arising from the ground state $I(^2P_{3/2})$ and spin−orbit excited $I(^2P_{1/2})$ iodine channels.[16]

The pulsed valve and both Nd:YAG lasers were synchronized at a repetition rate of 10 Hz using a home-made digital delay generator. The optimum time delay between the pump an probe lasers in the DMS-d_6 photodissociation experiments was found to be ≈10 ns. The pulsed molecular beam was triggered to have the laser pulses interacting with the early edge of the gas pulse plateau in order to minimize the formation of clusters, while still achieving an effective cooling of the internal degrees of freedom of the DMS-d_6 molecules.

III. Data Analysis

A. Recoil Velocity Distribution. The methodology followed to extract recoil velocity distributions of the fragments originating in the photodissociation of a given molecule in REMPI-TOF measurements has been described by different authors (for recent work, see for instance refs 17−19), and only those aspects relevant to the present study are discussed here.

The REMPI-TOF profiles are sensitive to the one-dimensional projection on the detection axis, v_Z, of the three-dimensional velocity vector of the neutral photofragments. For a direct two-body photodissociation process from an isotropically oriented parent molecule, the distribution of the velocity component along the detection axis for a single speed, v, of a given fragment can be expressed by

$$g(v_Z) \propto 1 + \beta_{eff}(\theta,\alpha)\, P_2\left(\frac{v_Z}{v}\right) \qquad (1)$$

where $P_2(x)$ denotes the second Legendre polynomial. The effective anisotropy parameter, $\beta_{eff}(\theta,\alpha)$, is related with the actual spatial anisotropy parameter β and with the fragment angular momentum alignment moments with respect to the recoil velocity through a complicated analytical expression,[19] which involves the angle between the electric field vector of the

dissociation laser and the detector axis, θ, and the angle between the electric field vectors of the dissociation and ionization lasers, α.

In the absence of angular momentum alignment of the fragments or if alignment effects are negligible, β_{eff} and β are related by the simple expression[19]

$$\beta_{eff} = \beta P_2(\cos\theta) \tag{2}$$

In such case, for a given speed distribution of the neutral fragments in the center-of-mass (CM) frame, $g(v)$, the projected velocity distribution on the detector axis observed experimentally is given by[17,18,20−22]

$$f(v_Z,\theta) = \int_{|v_Z|}^{v_{max}} \frac{g(v)}{2v}\left\{1 + \beta\, P_2(\cos\theta)\, P_2\left(\frac{v_Z}{v}\right)\right\} dv \tag{3}$$

where v_{max} is the maximum speed allowed by energy conservation.

The TOF profiles of the CD_3 fragment were measured tuning at the rotational Q-branch of the $4p_z$ 0_0^0 band. As pointed out recently by Eppink and Parker in velocity map imaging experiments on the photodissociation of ICH_3,[23,24] at the Q-branch of the 0_0^0 band of the CD_3 fragment alignment effects are much weaker than in the other branches. In our case, even if alignment effects still remain in the photodissociation of DMS-d_6, they are not sufficiently strong to cause significant changes in the CD_3^+ TOF profiles within the signal-to-noise ratio of our experiments as the probe laser polarization angle α was rotated.

The measured TOF profile is the result of the convolution of the instrumental response function over $f(v_Z,\theta)$ given by eq 3, where v_Z is related to the ion arrival time, t, by the following expression valid for space-focusing ion source conditions[26]

$$v_Z = \frac{q}{m}E_{ext}(t_0 - t) \tag{4}$$

where q/m is the charge-to-mass ratio of the detected ion, E_{ext} is the extraction electric field, and t_0 is the mean flight time of the ion.

The speed distribution $g(v)$ and the anisotropy parameter β were obtained from the simultaneous fit of TOF profiles measured at three different configurations, i.e., $\theta = 0°$, 54.7°, and 90°. The fit procedure begins with the analysis of the TOF profile measured at the magic angle, where the $P_2(\cos\theta)$ polynomial vanishes, thus resulting in a β-independent expression for the v_Z distribution:

$$f(v_Z,54.7°) = \int_{|v_Z|}^{v_{max}} \frac{g(v)}{2v}\, dv \tag{5}$$

The β parameter is finally determined from the fit of the measurements at $\theta = 0°$ and 90°, which also constitute a consistency check for the best-fit $g(v)$ distribution and for the methodology employed. We recall that β values for prompt axial recoil range from -1 (perpendicular dipole transition) to 2 (parallel dipole transition).

We have built the speed distribution, $g(v)$, from a CM recoil energy distribution, $P(E_{rec}/E_{max})$, modeled by a modified Gaussian function of the form

$$P(x) = Nx(1-x)\exp\left[-\left(\frac{x - x_0}{\Delta x}\right)^2\right], \quad x = E_{rec}/E_{max} \tag{6}$$

Hence

$$g(v) = N' u P(u^2), \quad u = v/v_{max} \tag{7}$$

In the above expressions, x and u represent the ratios of the fragment recoil energy and velocity, respectively, to the maximum values allowed by energy and momentum conservation, x_0 and Δx are fit parameters, and N, N' are normalization constants.

B. Rotational Populations of CD_3. Rotational state populations of nascent CD_3 have been determined from the measurement of the $4p_z$ 0_0^0 rotationally state-resolved 2+1 REMPI spectrum. If N'' and N' denote the rotational quantum numbers of the ground and intermediate resonant states, respectively, and K represents the projection of the rotational angular momentum vector on the C_3 symmetry axis of CD_3, the intensity of each $(N',K) \leftarrow (N'',K)$ REMPI rotational transition is given by

$$I_{N'N'',K} = F\frac{S_{N'N'',K}}{2N''+1}\frac{1}{D_{N',K}}P_{N'',K} \tag{8}$$

where $P_{N'',K}$ is the relative population of each (N'',K) rotational level of ground-state CD_3, including the nuclear spin degeneracy; $S_{N'N'',K}$ are the two-photon line-strength factors for each rotational transition,[27] and F is a global scaling factor. Finally, $D_{N',K}$ accounts for the predissociation of electronically excited CD_3, which for the $4p_z$ $^2A''_2$ state in the ground vibrational state is dominated by rotation-translation Coriolis coupling.[14]

Predissociation decreases the lifetime of the electronically excited states, which leads to a state-dependent loss of ionization efficiency of the form[14,28]

$$D_{N',K} = 1 + \frac{\Delta w_i}{\Delta w_h}[N'(N'+1) - K^2] \tag{9}$$

In addition, predissociation induces a natural frequency broadening Δw_n in the REMPI transitions which can be cast as[14]

$$\Delta w_n = \Delta w_h + \Delta w_i[N'(N'+1) - K^2] \tag{10}$$

where $\Delta w_h = 0.4$ cm^{-1} and $\Delta w_i = 0.012$ cm^{-1} define the homogeneous and heterogeneous predissociation line broadenings, respectively. Their values have been obtained from the best-fit of the widths of individual (N'',N',K) lines in the spectrum and are in good agreement with those obtained in previous REMPI experiments on the photodisociation of ICD_3.[14] Note that predissociation of CD_3 in the $4p_z$ state is much less important and has a smaller heterogeneous contribution than in the case of CH_3.[14,16]

Each individual transition was simulated with a peak of Lorentzian shape with full width at half-maximum (fwhm) Δw_n given by eq 10. The calculated spectrum was convoluted with a Gaussian function of fwhm $\Delta w_{exp} = 1$ cm^{-1} to account for the instrumental contributions to the measured line width.

The energies of the rotational levels of the $X^2A''_2$ ground state and the $4p_z$ $^2A''_2$ electronic excited state of CD_3 were calculated using the oblate symmetric-top expansion[29] with constants taken from ref 14.

We have evaluated the (N'',K) state distribution of the CD_3 fragment by means of a least-squares fit of the measured REMPI spectrum. The population distribution $P_{N''K}$ was expressed as

$$P_{N''K} = \rho(N'')\rho(K/N'') \tag{11}$$

where the overall population probabilities of the N'' states, $\rho(N'')$,

were taken as least-squares fit parameters. Three simple trial functions were used to represent the conditional probability distribution $\rho(K|N'')$ in order to describe different types of propensities for the orientation of the angular momentum of the CD_3 fragments:

$$\rho_1(K|N'') = C_{N''}G_K(1 + 2|K|/N'') \quad \text{(high } K \text{ values favored)} \quad (12)$$

$$\rho_2(K|N'') = C_{N''}G_K(3 - 2|K|/N'') \quad \text{(low } K \text{ values favored)} \quad (13)$$

$$\rho_3(K|N'') = C_{N''}G_K \quad \text{(no } K \text{ propensity)} \quad (14)$$

The nuclear spin degeneracy factor, G_K, is equal to 1 and 10 for N'' even and odd, respectively, and $K = 0$, whereas it follows the progression 8,8,11,8,8,11,..., for $|K| = 1,2,3,4,5,6,...(|K| \leq N'')$.[29] The constant $C_{N''}$ normalizes to unity the conditional distribution within each N''-manifold. For the analysis of the $4p_z$ 0_0^0 rotational spectrum of the ICD_3 photodissociation experiment, the only additional requirement was the conservation in the CD_3 fragment of the 11/16 ortho/para ratio of the parent molecule.[25]

Since K is a measure of the projection of the rotational angular momentum on the C_3 symmetry axis, the $\rho_1(K|N'')$ function given by eq 12 implies a tendency of the CD_3 fragment to rotate around an axis close to the C_3 one, whereas $\rho_2(K|N'')$ given by eq 13 corresponds to the preference for a "tumbling" rotation around an axis close to the CD_3 plane. The $\rho_3(K|N'')$ function of eq 14 describes products with uniform probability for all K values, except for the nuclear spin degeneracy.

In previous investigations on the photodissociation of ICD_3[28] and CH_3SCH_3,[8] a modified Boltzmann function was employed to model the rotational distribution $P_{N''K}$ of the CD_3 or CH_3 products in which the population of the K and N'' states was parametrized by means of two effective "temperatures" T_N and T_K in such a way that for $T_K > T_N$, $T_K < T_N$ or $T_K \approx T_N$, similar behaviors as those obtained by using the $\rho_i(K|N'')$, $i = 1,2,3$, functions of eqs 12−14, respectively, can be modeled. It is important to notice that, apart from the nuclear spin statistics, a true Boltzmann distribution would implicitly favor high K values within each N'' manifold, since the rotational energy $E(N'',K)$ is a decreasing function of K for an oblate symmetric top.

IV. Results and Discussion

A. Absorption Spectrum of Dimethyl Sulfide. Figure 1 shows the gas phase absorption spectrum of DMS measured in a low-resolution spectrophotometer at room temperature. The spectrum reproduces closely the features observed in higher resolution measurements by other groups.[1,9,10,12,30]

According to recent investigations based on magnetic circular dichroism,[9] the absorption of the molecule in the 214−230 nm range is assigned to the first dipole allowed transition 1^1B_1 ($9a_1 \leftarrow 3b_1$) $\leftarrow X^1A_1$, whereas at wavelengths shorter than 214 nm is associated with the more energetic transition $2^1B_1(10a_1 \leftarrow 3b_1) \leftarrow X^1A_1$.

As already mentioned, the focus of our experiments is on the photodissociation of CD_3SCD_3 at 229 nm, this wavelength lying on the red edge of the first absorption maximum (see Figure 1).

B. REMPI-TOF Spectra. Figure 2 depicts one-color TOF mass spectra produced by multiphoton ionization (MPI) of CD_3SCD_3 at the laser wavelengths 229 nm and 286.7 nm (Q-branch of the $4p_z$ 0_0^0 transition of CD_3) and different laser pulse energies (Figure 2a−c). The bottom panel (Figure 2d) displays the TOF spectrum obtained in a pump-probe experiment with overlaping 229 nm and 286.7 nm lasers. All these TOF spectra were recorded with the polarization of both lasers perpendicular to the TOF axis. Notice the different sensitivity of the mass spectra shown in the four panels.

The one-color mass spectra are dominated by the parent ion mass, in good agreement with similar measurements by Morgan et al.[31] As the laser intensity increases, the fragmentation of the parent ion becomes more extensive and the contribution of CD_3^+ and SCD_n^+ to the mass spectrum is considerably larger (see panel 2a in comparison with 2b).

The two-laser spectrum of Figure 2d was measured with a detection sensitivity 10 times lower than the single-laser mass

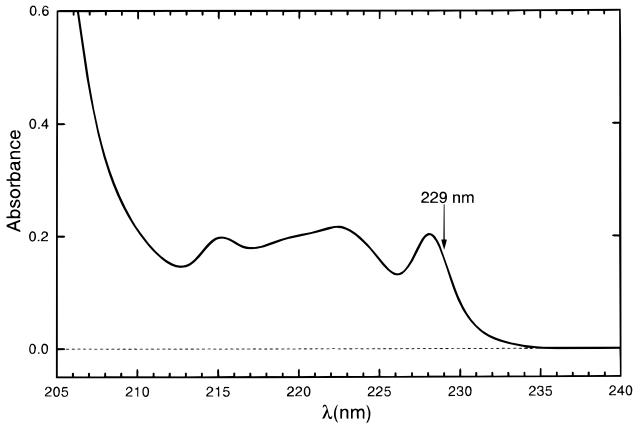

Figure 1. Gas phase absorption spectrum of dimethyl sulfide measured with a low resolution spectrophotometer. The arrow indicates the excitation wavelength of the present photodissociation study.

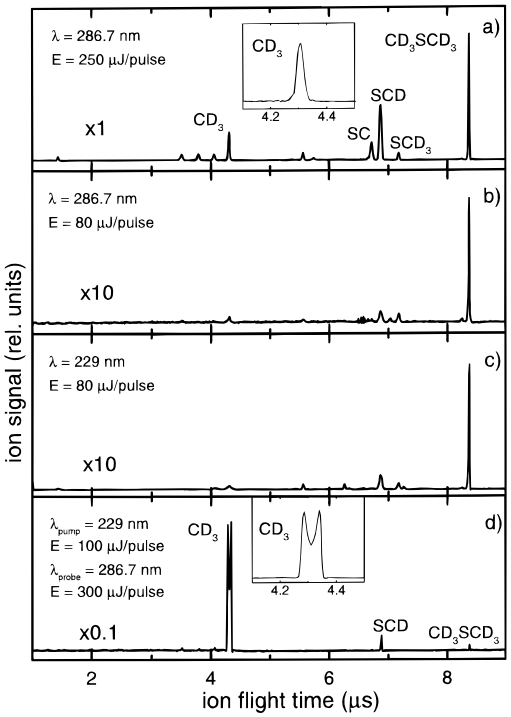

Figure 2. Time-of-flight mass spectra obtained from the multiphoton ionization of CD_3 SCD_3 with single laser pulses at 286.7 nm (panels a and b) and 229 nm (panel c) and with two overlapping, 10 ns time delayed lasers at 229 and 286.7 nm wavelengths (panel d). The scale in panel d is 10^2 times greater than those in panels b and c and 10 times greater than in panel a.

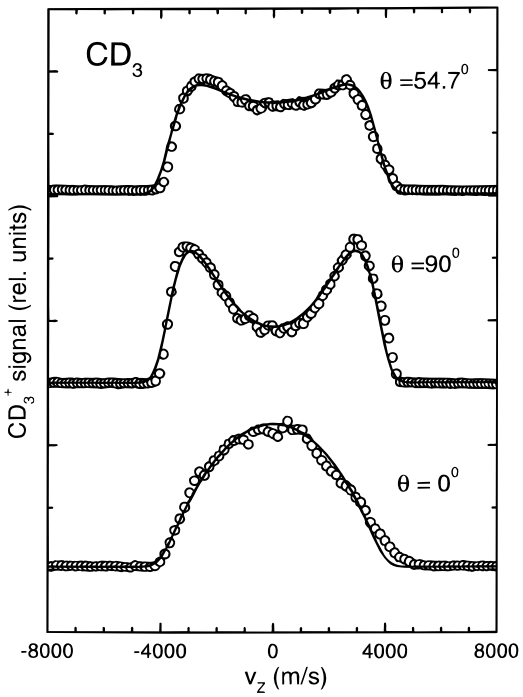

Figure 3. REMPI-TOF profiles (open circles) of the CD_3 fragments originated in the photodissociation of CD_3SCD_3 at 229 nm measured in the Q-branch of the $4p_z\ 0_0^0$ band at three different angles between the dissociation laser polarization and the TOF detector axis, $\theta = 54.7°$ (upper), 90° (middle), and 0° (bottom). The solid curves through the symbols represent the best-fit simulations to the measured TOF profiles. See text for details.

spectrum of panel 2a (notice the weaker MPI signal at the SCD^+ and parent ion masses). The intense CD_3^+ resonant peak observed in the spectrum becomes negligible in this scale when either the pump or probe laser is turned off. In contrast to the single peak observed for this fragment ion in the one-color spectra (see inset in Figure 2a), the pump−probe TOF CD_3^+ peak displays a double-maximum structure (inset in Figure 2d) characteristic of the spatial anisotropy of the CD_3 fragments originated in the photodissociation of DMS-d_6 (see below).

We have measured the dependence of the CD_3^+ signal with the pump and probe laser energies. The ion signal varies linearly with the dissociation laser energy and shows a quadratic dependence with the probe laser energy, as expected for a 2+1 REMPI process.

C. Fragment Recoil Energy Distribution and Anisotropy Parameter. The angular and recoil velocity distribution of the products originating in the photodissociation of CD_3SCD_3 at 229 nm was investigated by measuring TOF profiles of the $CD_3(v=0)$ fragments on the Q-branch of the $4p_z\ 0_0^0$ band. TOF profiles were taken with the pump laser polarization at three different angles with respect to the TOF axis, namely, $\theta = 0°$, 54.7°, and 90°, and the probe laser polarization was kept perpendicular to the TOF axis. In addition, the detection at the broad Q-branch of CD_3 favors that all velocity groups are observed with the same sensitivity. Special care was taken in the measurements to ensure that the Q-branch signal was not saturated.

Figure 3 shows the experimental CD_3 TOF profiles recorded for the three pump laser polarizations together with the corresponding best-fit simulations. As can be seen, the two-parameter $g(v)$ function given by eq 7 and a simple anisotropy parameter β provide a satisfactory fit to the measured profiles (see section IIIA).

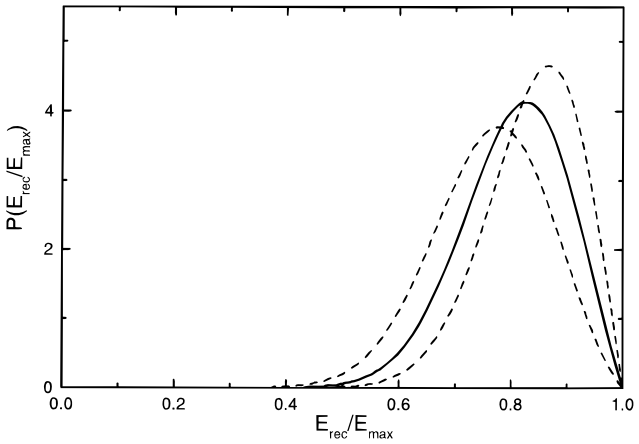

Figure 4. Best-fit recoil energy distribution $P(E_{rec}/E_{max})$ (solid curve) for the 229 nm photodissociation of CD_3SCD_3 as a function of the ratio between the recoil energy, E_{rec}, and the maximum energy available, E_{max}. The distributions given by the dashed curves still provide an acceptable fit to the REMPI-TOF profiles and represent the uncertainty of the distribution. See text for details.

The analysis of the TOF profiles yields a best-fit anisotropy parameter $\beta = -0.9 \pm 0.1$. This value, which is very close to the limiting value −1, indicates that the dissociating absorption of CD_3SCD_3 at 229 nm is predominantly associated with a pure perpendicular dipole electronic transition, and hence the observed anisotropy parameter is consistent with the previous assignment of the transition $1^1B_1 \leftarrow X^1A_1$ as being responsible for the first absorption band of DMS.[1,9−12]

Figure 4 depicts the best-fit CM recoil energy distribution $P(E_{rec}/E_{max})$ (eq 6) of the $CD_3(v=0)$ products. The dashed curves in the figure denote distributions that still provide a reasonable fit to the three TOF spectra of Figure 3 and illustrate the uncertainty that affects the present determination. Note that the CM energy distribution represented in Figure 4 can be interpreted from momentum conservation as either CD_3 recoil energy ($E_{max}(CD_3) = 152.5$ kJ/mol), CD_3S recoil energy ($E_{max}(CD_3S) = 54.9$ kJ/mol), or as relative recoil energy for the $SCD_3 + CD_3$ fragments ($E_{max}(CD_3S-CD_3) = 207.4$ kJ/mol).

The best-fit recoil distribution shown in Figure 4 yields an average energy fraction $\langle x \rangle = \langle E_{rec}/E_{max} \rangle \approx 0.8$, which indicates that a substantial amount of the energy release in the CD_3SCD_3 dissociation is channeled into product translational energy of the fragments. This value is significantly larger than that obtained in previous CH_3SCH_3 photodissociation experiments at the shorter wavelength of 193 nm,[6,7] where, without final state selection in the methyl fragment, an average value of $\langle x \rangle = 0.6$ was obtained.

D. Rotationally State-Resolved CD_3 REMPI Spectra. We have investigated the rotational state distribution of the $CD_3(v=0)$ fragments produced in the 229 nm photodissociation of CD_3SCD_3 by measuring the $4p_z\ 0_0^0$ band. A typical REMPI spectrum is shown in Figure 5 along with the best-fit simulation obtained following the procedure outlined in section IIIB.

A series of scans were carried out at several configurations of the probe laser polarization, and no systematic effects on the relative intensities of the lines of the different branches were observed. These results indicate that angular momentum alignment has a weak effect on the determination of the rotational populations of the CD_3 fragments from the measured REMPI spectrum.

The Q-branch in the spectrum of Figure 5 is largely enhanced due to the $\Delta K = 0$ selection rule for a parallel two-photon transition and to the congestion of rotational states and favorable

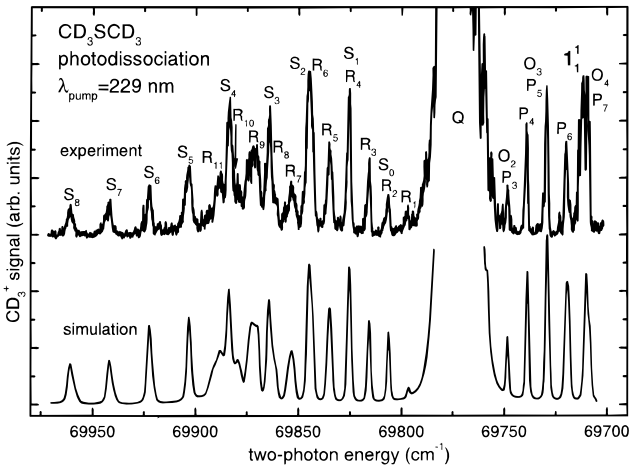

Figure 5. Top: measured 2+1 REMPI spectrum of the $4p_z\ 0_0^0$ band of the $CD_3(v=0)$ fragments arising from the photodissociation of DMS-d_6 at 229 nm. Rotationally state-resolved lines are observed at both sides of the intense Q-branch and are assigned to the two-photon allowed O, P, R, and S $N' \leftarrow N''$ branches as indicated. The 1_1^1 vibrational band of the ν_1 stretching mode is also observed. Bottom: least-squares simulation obtained as described in section IIIB using the K-state distribution $\rho_3(K|N'')$ of eq 14.

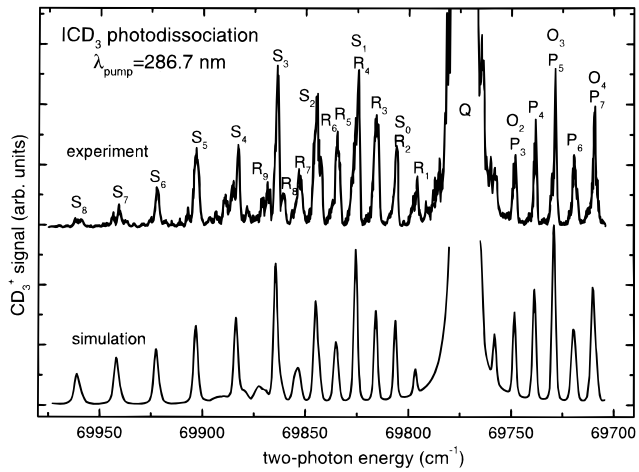

Figure 6. Same as Figure 5 but for the one-color photodissociation ($\lambda_{pump} = \lambda_{probe} = 285.7-287$ nm) of ICD_3 into $I(^2P_{1/2}) + CD_3(v=0)$ products. The least-squares simulation shown at the bottom of the figure was calculated with the *K*-state distribution $\rho_2(K|N'')$ of eq 13.

line strengths.[27] In addition, O, P, R, and S resolved transitions from product rotational states with $N'' = 0-12$ are neatly observed within the two-photon energy interval covered by the measurement. The spectrum presents relatively intense R_6-R_{12} lines at 69 840−69 900 cm^{-1}, which indicates that states with $N'' = 6-12$ receive an important fraction of the population. These REMPI lines are also broader than those associated with lower rotational states due to the larger number of *K* states contributing to the N'' manifold.

The production of rotationally excited $CD_3(v=0,N''=6-12)$ corresponds to a transfer of as much as ≈9 kJ/mol of the available energy to rotational energy of the fragment. Although this constitutes a relatively small fraction of the total available energy (≈4%), it is significantly larger than that observed in other photoinitiated processes yielding CD_3, such as the photodissociation of ICD_3[16] or the $Cl + CD_4$ reaction.[32]

In order to compare more rigorously the present results with the benchmark ICD_3 A-band photodissociation,[16,24,25] we have performed single laser experiments with this molecule ($\lambda_{pump} = \lambda_{probe} \approx 286.7$ nm). The $CD_3(v=0)$ REMPI spectrum for the predominant dissociation channel yielding spin−orbit excited $I(^2P_{1/2})$ formation is depicted in Figure 6. This spectrum shows significant differences with respect to that obtained for DMS-d_6 (Figure 5). As can be seen, the lines associated with the highest N'' states are much less intense, especially the R_6, R_9, and R_{11} lines. In contrast, the relative intensity of lines associated with the lowest N'' states, such as the R_1, R_2, R_3, or the S_3 are markedly larger. Therefore, the N'' state population distribution of the CD_3 fragments arising from the photodissociation of ICD_3 appears to be significantly cooler than that from the photodissociation of CD_3SCD_3.

From the best-fit simulations of the spectra shown in Figures 5 and 6, we have obtained rotationally state-resolved distributions of the $CD_3(v=0)$ products. As discussed below in more detail, the conditional *K*-state distribution functions $\rho_3(K|N'')$ and $\rho_2(K|N'')$ provide the best overall fit to the measured spectra for CD_3SCD_3 and ICD_3, respectively. The resulting least-squares N''-state population probabilities, $\rho(N'')$, for the CD_3 fragments are shown in Figure 7. Notice that $\rho(N'')$, as defined by eqs 11−14, includes implicitly the $2N'' + 1$ rotational degeneracy.

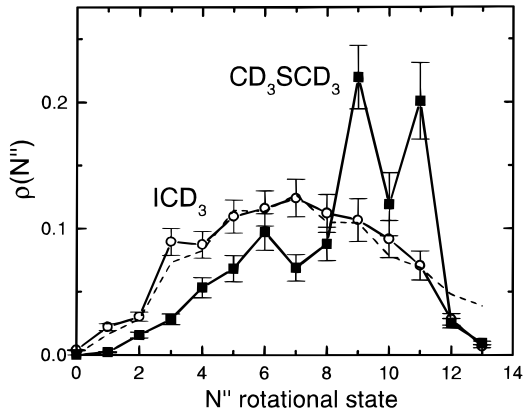

Figure 7. N'' rotational distributions of the $CD_3(v=0)$ products originating in the photodissociation of CD_3SCD_3 at 229 nm (squares) and in the photodissociation of ICD_3 at 286.7 nm (circles) obtained from the best-fit simulations shown at the bottom of Figures 5 and 6, respectively. The latter rotational distribution is compared with that obtained from the two-temperature model using $T_N = 400$ K and $T_K = 200$ K (dash line).

As can be seen in Figure 7, nascent $CD_3(v=0)$ fragments from the photodissociation of DMS-d_6 show a rotational state distribution biased toward the larger quantum states observed ($N'' = 9-11$). The anomalously small probability at $N'' = 10$ resulting from the least-squares fit in comparison to the neighbor rotational states $N'' = 9$, 11 is related to an actual lack of intensity of the R_{10}. This result is, however, to some extent uncertain due to the partial overlap of the R_{10} and R_{11} lines with the more intense S_4 line.

In contrast, the $CD_3(v=0)$ fragments originated in the photodissociation of ICD_3 at ≈286.7 nm show a broad and smooth rotational distribution peaking at $N'' = 6-8$. This distribution can be well reproduced with the modified Boltzmann functionality used in previous studies,[28] with fit parameters $T_N = 400$ K and $T_K = 200$ K (dash line in Figure 7). These values of T_N and T_K are somewhat larger than those obtained in ref 28 for the dissociation of ICD_3 in a molecular beam with CD_3 detection via the $3p_z$ band.

The average rotational energies of the $CD_3(v=0)$ products are 330 cm^{-1} (4.0 kJ/mol) and 255 cm^{-1} (3.0 kJ/mol) for DMS-d_6 and ICD_3, respectively, which in both cases represent ≈2% of the total available energy. Therefore, in average, the relative

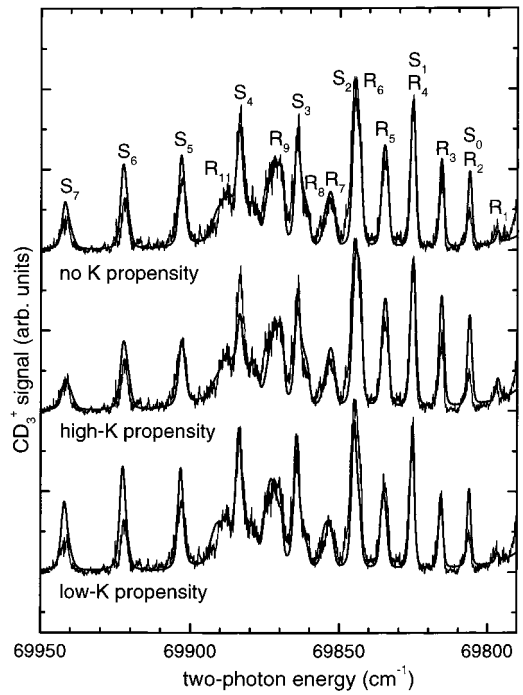

Figure 8. Comparison of the CD_3 REMPI spectrum measured in the photodissociation of CD_3SCD_3 at 229 nm with the least-squares simulated spectra obtained by using the three *K*-state distributions $\rho_3(K|N'')$ (top), $\rho_1(K|N'')$ (middle), and $\rho_2(K|N'')$ (bottom). See text for details.

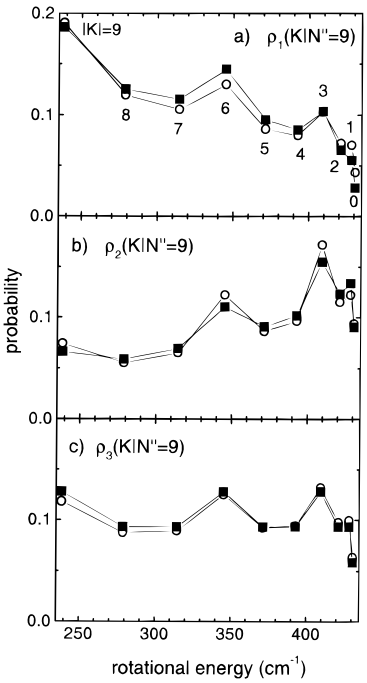

Figure 9. *K*-state distributions for the $N'' = 9$ rotational state from the three models used in the present work (eqs 12−14). Top: $\rho_1(K|N'')$ (solid squares) and a Boltzmann distribution at $T_N = 400$ K (open circles). Middle: $\rho_2(K|N'')$ (squares) and a two-temperature model distribution with $T_N = 400$ K and $T_K = 20$ K (circles). Bottom: $\rho_3(K|N'')$ (squares) and a two-temperature distribution with $T_N = 400$ K and $T_K = 400$ K (circles). The distributions $\rho_3(K|N'')$ and $\rho_2(K|N'')$ provide the best-fit to the CD_3 REMPI spectra measured in the CD_3SCD_3 (Figure 6) and ICD_3 (Figure 7) photodissociation, respectively.

efficiency for CD_3 rotational excitation is similar in the photodissociation of both molecules.

We concentrate now on the analysis of the *K*-state envelopes and intensities of the S and, especially, the R branches in the measured DMS-d_6 REMPI spectrum. Figure 8 depicts three different least-squares fits of the REMPI spectrum in the range 69 950−69 800 cm^{-1}, each one obtained by assuming a different propensity for the *K*-state population distribution: $\rho_1(K|N'')$ (high *K* values favored, i.e. C_3 rotation), $\rho_2(K|N'')$ (low *K* values favored, i.e. "tumbling" rotation) and $\rho_3(K|N'')$ (no *K* propensity). In particular, for $N'' = 9$, one of the most populated and best resolved states, the three best-fit distributions $\rho_i(K|N'')$, $i = 1, 2, 3$, are shown in Figure 9. The $\rho_1(K|N'')$ distribution is compared with a Boltzmann distribution at $T = 400$ K, whereas the $\rho_2(K|N'')$ and $\rho_3(K|N'')$ distributions are compared with those obtained using the two-temperature model of refs 8 and 28 with parameters $T_N = 400$ K, $T_K = 200$ K, and $T_N = T_K = 400$ K, respectively.

The spectrum shown in the upper part of Figure 8 was simulated using the model distribution $\rho_3(K|N'')$, which corresponds to a uniform probability distribution for all states $K = -N''$, ... , N'' (except for the nuclear spin degeneracy). This particular function seems to provide the best overall fit to the measured spectrum, and, in particular, it reproduces satisfactorily the *K*-state envelope of the best resolved lines, such as R_9 and R_{11}. The fits obtained by using $\rho_1(K|N'')$ and $\rho_2(K|N'')$ are somewhat less satisfactory. The $\rho_1(K|N'')$ model, favoring the higher *K* values (middle curve in Figure 8), yields a good fit for the higher N'' lines, except for a too narrow R_9 line shape in comparison with experiment, but underestimates the relative intensity of several low N'' lines, e.g. the S_3 and S_4 lines. The low *K* propensity $\rho_2(K|N'')$ model (lower curve) fits best the lower N'' states but yields a worse fit for the high N'', leading to a slight but appreciable shift of the R_7-R_{11} lines toward greater energies and also to an overestimation of the $S_{N''}/R_{N''}$ intensity ratios for $N'' = 5-7$.

In our previous study on the photodissociation of CH_3SCH_3 at 227.5 nm in a molecular beam,[8] the analysis of the CH_3 REMPI spectrum showed that a modified Boltzmann function with temperatures $T_N = 325$ K and $T_K = 125$ K produced the best-fit simulation, indicating a preference for rotation of the CH_3 fragment around an axis perpendicular to the C_3. In the present work, we have analyzed the CH_3 REMPI spectrum obtained in the photodissociation of CH_3SCH_3 at 229 nm (not shown), measured exactly in the same experimental conditions as the one for DMS-d_6, and we have found that the low *K* propensity distribution $\rho_2(K|N'')$ provides the best-fit simulation to the measured spectrum. It must be noted, however, that the $4p_z$ Rydberg state of CH_3 is subject to a much larger predissociation than that of CD_3 as N' increases. Therefore, the CH_3 REMPI spectrum is made of only a few lines from states with $N'' \leq 4$[8] and yields little or no information about the population of the higher N'' states.

In summary, from the above considerations it seems that a population distribution with no *K* propensity is more adequate to simulate the DMS experimental data for the higher rotational states $N'' \geq 5$ of the $CD_3(v=0)$ photofragments, whereas the low *K* propensity model describes better the lines of the lowest rotational states. This apparent difference in the population of the *K* levels for the high N'' states in comparison to the low N'' states might indicate dynamical differences in the photodissociation process in each case.

Previous experiments on the A-band photodissociation of ICD_3 cooled in a molecular beam agree with our observation that the CD_3 fragment is produced predominantly in low *K* states.[25,33−35] This is confirmed by the analysis of our CD_3 REMPI spectrum of Figure 6 where the simulation performed

with the low K propensity distribution $\rho_2(K|N)$ (also shown in Figure 6) provides the best overall fit to the experiment.

The DMS-d_6 molecules in the present experiments were cooled in a free jet under similar conditions as ICD_3. Therefore, we can rule out the possibility that the population of high K levels in the largest N'' states of the nascent CD_3 that originated in the photodissociation of DMS-d_6 emerges from the conservation of the initial rotation of the methyl group in the parent molecule, as found previously for warm ICD_3 prepared in an effusive leak.[16]

E. Vibrational Excitation of CD_3. In a recent experiment in our group on the photodissociation of CH_3SCH_3 at 227.5 nm,[8] CH_3 products with up to four quanta of vibrational excitation in the ν_2 "umbrella" mode were detected. It became apparent that a significant amount of energy is channeled toward the ν_2 mode and, possibly, to other undetected modes. However, no activity of the ν_1 "symmetric stretch" mode could be observed within the signal-to-noise ratio of the REMPI measurements, although the spectral region accessible to the experiments included the 1_1^1 $3p_z$ REMPI transition at $\approx$59 898 cm^{-1}, detected by Eppink and Parker[24] in the CH_3 fragment from the dissociation of ICH_3 associated with the production of $I(^2P_{3/2})$.

The present investigation does provide evidence for activity in the ν_1 mode of the CD_3 fragment of CD_3SCD_3. As can be seen in Figure 6, a differentiated $4p_z$ 1_1^1 band is observed in the CD_3 REMPI spectrum at $\approx$69 710 cm^{-1} with an intensity comparable to the most intense rotational transitions of the 0_0^0 band. Interestingly, the detected 1_1^1 band intensity is of similar magnitude to that observed in the $I(^2P_{3/2}) + CD_3$ channel of the A-band photodissociation of ICD_3 (not shown), in agreement with what was found in ref 16. In contrast, no ν_1 activity is observed in the $I(^2P_{1/2}) + CD_3$ channel yielding spin−orbit excited iodine (see Figure 7), in accordance with previous works.[16,24]

F. Energy Disposal and Dynamics of the Photodissociation of CD_3SCD_3. From the results and analysis discussed above for the photodissociation of CD_3SCD_3 yielding $CD_3(v=0)$ products, we conclude that about 80% of the available energy appears as translational energy of the fragments, whereas only about 2% appears as rotational energy of $CD_3(v=0)$. Thus, the remaining 18% of the available energy (i.e., 37 kJ/mol) is channeled into rovibrational energy of the CD_3S fragment in the electronic ground state. This is in agreement with the considerations presented in our previous investigation on the photodissociation of CH_3SCH_3,[8] in which, in addition, a low vibrational excitation of the CH_3 ν_2 umbrella mode was also observed (ca. <5% of the available energy). Therefore, the dynamics of the photodissociation of dimethyl sulfide on the first absorption band seems to imply an inefficient internal excitation of the nascent methyl fragment and a preferential channeling of the available energy into recoil translation of the fragments and, to a less extent, into the internal modes of CD_3S.

Within the C_s symmetry, the 229 nm dissociation of DMS takes place via a superposition of the $1^1A''$ and $2^1A''$ electronic states which become coupled by the initial excitation of the C−S−C asymmetric stretch in the parent molecule.[13] Although the $2^1A''$ state cannot dissociate adiabatically upon absorption at 229 nm, it can decay into the ground state fragments $CH_3(X^2A') + CH_3S(X^2E)$ via the conical intersection of both $^1A''$ excited states. Second-order CI-SCF calculations by Manaa and Yarkony[13] indicate that the region of conical intersections is located within the Franck−Condon range of the transition and that it involves excitation of the C−S−C asymmetric stretch, eventually leading to an impulsive breaking of the C−S bond of the DMS parent molecule, and thus to a large translational excitation of the fragments. In fact, as pointed out in section IVC, the energy disposal into product translation is larger at 229 nm than that found in previous experiments at 193 nm.[6,7] The higher complexity of the excited states accessed at 193 nm, presumably mainly a $^1A_1$ state,[9] allows for a more effective coupling to the internal energy of the fragments in comparison with the more direct dissociation process which takes place on the first absorption band.

A similar situation has been found in previous experiments on the photodissociation of H_2S on the first absorption band, which yields HS fragments with little vibrational and rotational excitation.[36] In H_2S, as in DMS, the first dipole-allowed transition excites the molecule to the 1^1B_1 excited state, which, as the S−H bonds stretches, strongly mixes with the 1^1A_2 state (both $^1A''$ states in C_s symmetry).[37] The calculations of Manaa and Yarkony[13] for CH_3SCH_3 show that the C−S−C angle changes from 105.5° (equilibrium value in the ground state) to $\approx$112° (in the vicinity of the conical intersection). In addition, the S−C−H angle varies significantly, which suggests that geometrical changes in the CH_3S fragment may play an important role when the surface of conical intersection is reached, implying internal excitation in this fragment.

The rotational distributions of $CD_3(v=0)$ obtained from the photodissociation of DMS-d_6 (perpendicular transition) is sensibly hotter than that obtained from ICD_3 (parallel transition). However, on average, the amount of rotational excitation of the fragment is similar for both molecules. Therefore, it seems that the DMS photolysis mimics the prompt $I-CH_3$ bond-breaking process as far as the transfer into translational energy of the fragments is concerned and in spite of the different geometries and mass ratios involved in each system. However, the propensity observed for alignment of the CD_3 rotational angular momentum vector perpendicular to the C_3 axis in the photodissociation of ICD_3 is not so clear in DMS-d_6.

V. Conclusions

In this work, the photodissociation of the fully deuterated isotopic variant of dimethyl sulfide, CD_3SCD_3, from the lowest dipole-allowed transition 1^1B_1 ($9a_1 \leftarrow 3b_1$) $\leftarrow X^1A_1$ was studied at 229 nm. The REMPI-TOF technique was exploited to characterize the angular and recoil energy distributions of the nascent CD_3 fragment. In addition, the rotational distribution of $CD_3(v=0)$ was obtained from the analysis of the rotationally state-resolved $4p_z$ 0_0^0 2+1 REMPI spectrum.

The analysis of the measured CD_3 TOF profiles yields an anisotropy parameter of $\beta = -0.9 \pm 0.1$, close to the limiting value of -1 for a pure perpendicular dipole transition, and an average value of the fragment recoil energy of 80%, sensibly larger than that obtained in previous experiments on the photodissociation of DMS at 193 nm (60%).

In DMS-d_6, the $CD_3(v=0)$ rotational distribution obtained from the analysis of the REMPI spectra peaks at the largest N'' values, in strong contrast with the same distribution measured in the photodissociation of ICD_3 at $\approx$286.7 nm, which peaks at $N'' = 6-8$. However, on average, the amount of the total available energy that appears as rotational energy of the CD_3 fragment is very similar for both molecules.

A detailed analysis of the K-state envelopes and intensities of the different N'' lines in the rotationally resolved $CD_3(v=0)$ REMPI spectrum arising from the photodissociation of DMS-d_6 reveals that a population distribution with no K-state propensity is the one which reproduce best the measured spectrum for the larger N'' states, whereas a low K propensity

distribution is the more adequate for the lowest N'' states, the latter in agreement with our previous study on the photodissociation of CH_3SCH_3. This is, however, at variance with a similar analysis of the $CD_3(v=0)$ fragments arising from the photodissociation of ICD_3, in which the best-fit simulation of the $CD_3(v=0)$ REMPI spectrum is obtained using a low K propensity population distribution for all N'' states.

Acknowledgment. B.M.-H. acknowledges financial support from the program "Acciones para la Incorporación de Doctores y Tecnólogos" of the Ministry of Education and Culture of Spain. We acknowledge the facilities provided by the CAI de Espectroscopía-Servicio de Espectroscopía Multifotónica (REMPI) of the Universidad Complutense de Madrid. This project was financed by the DGICYT of Spain (grant no. PB98-0762-C03-01).

References and Notes

(1) Thompson, S. D.; Carrol, D. G.; Watson, F.; O'Donnell, M.; McGlynn, S. P. *J. Chem. Phys.* **1966**, *45*, 1367.
(2) Lee, J. H.; Timmons, R. B.; Stief, L. J. *J. Chem. Phys.* **1976**, *64*, 300.
(3) Sheraton, D. F.; Murray, F. E. *Can. J. Chem.* **1981**, *59*, 2750 and references therein.
(4) Calear, A. B.; Dixon, D. R. *Trans. Faraday Soc.* **1970**, *67*, 1987.
(5) Rao, P. M.; Knight, A. R. *Can. J. Chem.* **1972**, *50*, 844.
(6) Nourbakhsh, S.; Norwood, K.; Yin, H. M.; Liao, C. L.; Ng, C. Y. *J. Chem. Phys.* **1991**, *95*, 5014.
(7) Lee, Y. R.; Chiu, C. L.; Lin, S. M. *J. Chem. Phys.* **1994**, *100*, 7376.
(8) Martínez-Haya, B.; Zapater, I.; Quintana, P.; Menéndez, M.; Verdasco, E.; Santamaría, J.; Bañares, L.; Aoiz, F. *J. Chem. Phys. Lett.* **1999**, *311*, 159.
(9) Mason, W. R. *J. Chem. Phys.* **1996**, *100*, 8139.
(10) Clark, L. B.; Simpson, W. *J. Chem. Phys.* **1965**, *43*, 3666.
(11) Allkins, J. R.; Hendra, P. J. *Spectrochim. Acta* **1966**, *22*, 2075.
(12) McDiarmid, R. *J. Chem. Phys.* **1974**, *61*, 274.
(13) Manaa, M. R.; Yarkony, D. R. *J. Am. Chem. Soc.* **1994**, *116*, 11444.
(14) Black, J. F.; Powis, I. *J. Chem. Phys.* **1988**, *89*, 3986.
(15) Aoiz, F. J.; Díez-Rojo, T.; Herrero, V. J.; Martínez-Haya, B.; Menéndez, M.; Quintana, P.; Ramonat, L.; Tanarro, I.; Verdasco, E. *J. Phys. Chem. A* **1999**, *103*, 823.
(16) Powis, I.; Black, J. F. *J. Phys. Chem.* **1989**, *93*, 2461.
(17) Bergmann, K.; Carter, R. T.; Hall, G. E.; Huber, R. *J. Chem. Phys.* **1998**, *109*, 474 and references therein.
(18) McGivern, W. S.; Li, R.; Zou, P.; North, S. W. *J. Chem. Phys.* **1999**, *111*, 5771 and references therein.
(19) Mons, M.; Dimicoli, I. *J. Chem. Phys.* **1989**, *90*, 4037.
(20) Zare, R. N. *Mol. Photochem.* **1972**, *4*, 1.
(21) Dixon, R. N. *J. Chem. Phys.* **1986**, *85*, 1866.
(22) Cheng, P. Y.; Zhong, D.; Zewail, A. H. *J. Chem. Phys.* **1996**, *105*, 6216.
(23) Eppink, A. T. J. B.; Parker, D. H. *J. Chem. Phys.* **1998**, *109*, 4958.
(24) Eppink, A. T. J. B.; Parker, D. H. *J. Chem. Phys.* **1999**, *110*, 832.
(25) Janssen, M. H. M.; Parker, D. H.; Sitz, G. O.; Stolte, S.; Chandler, D. W. *J. Phys. Chem.* **1991**, *95*, 8007.
(26) Syage, J. A. *J. Chem. Phys.* **1996**, *105*, 1007.
(27) Chen, K.; Yeung, E. S. *J. Chem. Phys.* **1978**, *69*, 43.
(28) Chandler, D. W.; Janssen, M. H. M.; Stolte, S.; Strickland, R.; Thoman, J. W., Jr.; Parker, D. H. *J. Phys. Chem.* **1990**, *94*, 4839.
(29) Herzberg, G. *Molecular Spectra and Molecular Structure*; Van Nostrand Reinhold Co.: New York, 1966; Vol. III, p 94ff.
(30) Scott, J. D.; Causley, G. C.; Russell, B. R. *J. Chem. Phys.* **1973**, *59*, 6577.
(31) Morgan, R. A.; Orr-Ewing, R. A.; Ashfold, M. N. R.; Buma, W. J.; Wales, N. P. L.; de Lange, C. A. *J. Chem. Soc., Faraday Trans* **1995**, *91*, 3339.
(32) Kandel, S. A.; Zare, R. N. *J. Chem. Phys.* **1998**, *109*, 9719.
(33) Ogorzalek Loo, R.; Haerri, H. P.; Hall, G. E.; Houston, P. L. *J. Chem. Phys.* **1989**, *90*, 4222.
(34) Kim, D. Y.; Brandstater, N.; Pipes, L.; Garner, T.; Baugh, D. *J. Phys. Chem.* **1995**, *99*, 4364.
(35) Pisano, P. J.; Cline, J. I. *J. Chem. Phys.* **2000**, *112*, 6190.
(36) Schinke, R. *Photodissociation dynamics*; Cambridge University Press: Cambridge, UK, 1993, and references therein.
(37) Wilson, S. H. S.; Howe, J. D.; Ashfold, M. N. R. *Mol. Phys.* **1996**, *88*, 841.